Design of a Rear BLI Non-Axisymmetric Propulsor for a Transonic Flight Experiment

Andrea Battiston* and Rita Ponza†
HIT09 S.r.l., Padova, 35137, Italy

Ernesto Benini‡
University of Padova, Padova, 35131, Italy

Nowadays, the increasing demand for reducing the environmental impact of civil aviation is leading to more sustainable aircraft technologies. In the context of aircraft propulsion, Boundary Layer Ingestion (BLI) is considered one of the most promising solutions, although the high level of integration between the airframe and propulsors becomes a major challenge in the design process. The present work deals with a CFD based shape optimization of a BLI-360 propulsor, starting from a simplified two-dimensional axisymmetric model as a basis for the three-dimensional design.

I. Nomenclature

F	=	gauge force
ϕ	=	wall force acting on the drag domain
θ	=	wall force acting on the thrust domain
D_{ref}	=	reference fuselage drag of a non-BLI configuration
NAF	=	net assembly force and
ΔNAF	=	net assembly force referred to the reference drag
PSC	=	power saving coefficient
S_w	=	wall surface area
A	=	flow passage area
k	=	specific heats ratio
R	=	gas constant
T	=	static temperature
T^0	=	total temperature
p	=	static pressure
p^0	=	total pressure
ρ	=	density
M	=	Mach number
Re	=	Reynolds number
V	=	velocity
τ_w	=	wall shear stress
π_c	=	fan total pressure ratio
η_{pol}	=	fan polytropic efficiency
W_{fan}	=	fan shaft power
$W_{\Delta NAF}$	=	ΔNAF useful power
$\eta_{\Delta NAF}$	=	ΔNAF efficiency
$(\,)_\infty$	=	generic quantity evaluated at freestream conditions
$(\,)_I$	=	generic quantity evaluated at the propulsor fan intake section
$(\,)_E$	=	generic quantity evaluated at the propulsor fan exhaust section

*Research Engineer.
†Senior Research Engineer.
‡Professor, Department of Industrial Engineering, AIAA Member.

dv	=	design variables
BLI	=	Boundary layer ingestion
CFD	=	Computational Fluid Dynamics
RANS	=	Reynolds-Averaged Navier-Stokes
WTT	=	Wind Tunnel Test
MOOP	=	Multi-Objective Optimization Problem

II. Introduction

RECENTLY, a higher awareness about the environmental impact of civil aircraft transportation is leading to increasingly efforts for reducing fuel consumption. In such context, boundary layer ingesting systems are one of the most promising solutions, as a closer integration between fuselage and propulsors is considered a key in the achievement of more sustainable architectures. The concept of boundary layer ingestion is actually not new.

Applications in marine propulsion are quite common, and extensions to aeronautic propulsion have been considered in the past years[1]. At a conceptual level, the key to such technology is the wake filling principle (sketched in Figure 1) : the aircraft wake is re-energized as a consequence of the ingestion of the low-momentum boundary layer flow of the fuselage, thus providing a reduction in terms of momentum deficit and therefore a reduction of the jet velocity necessary to obtain the desired thrust, which eventually increases the propulsive efficiency.

Multiple BLI layouts have been proposed, such as the propulsive fuselages (PF), rear engines (RE) or distributed fans over blended wing body (BWB) concepts[2]. In this regard, although more integrated solutions as the BWB concepts appear more promising, concepts as the PF are most likely to be implemented within a shorter term due to a relatively small modification requirement to the classic tube and wing airframe.

At a more quantitative level, it is apparent that a BLI system design must undergo a refined optimization process in order to get a net benefit in terms of propulsive efficiency. Another challenge in the BLI propulsion analysis is the quantification of a consistent bookkeeping methodology and performance metrics.

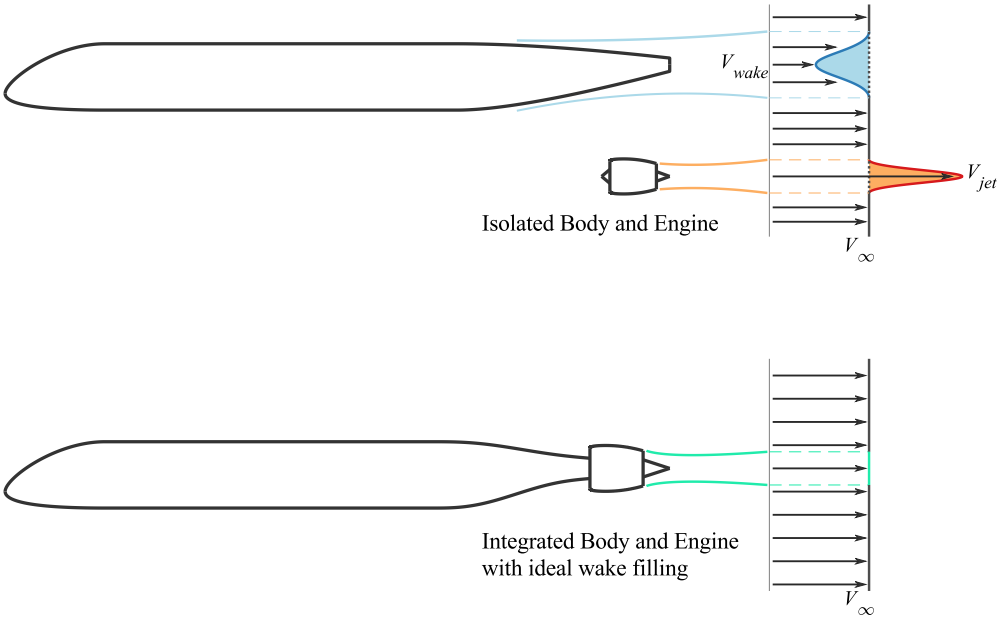

Fig. 1 Sketch of the wake filling principle.

In the present work, a design optimization process of a PF concept is presented, as part of an activity funded under the Clean Sky 2 Joint Undertaking Initiative of the European Union, under the SUBLIME project, which aims at understanding boundary layer ingestion and demonstrating the capabilities of these new propulsion systems to meet the goals set by ACARE for 2035. SUBLIME relies on both high-fidelity computational fluid dynamics and wind-tunnel testing at transonic regimes to assess the behavior of aircraft architectures suitable for appropriate propulsor installation which minimizes inlet flow distortions and maximizes power saving.

III. Scope of the Activity

One of the major concerns in the quantification of a BLI propulsor benefit is the definition of consistent performance metrics and references. In this regard, defining the thrust is not a simple task: the close integration between the propulsor and the airframe does not allow a clear separation between thrust and drag forces. Thus, various bookkeeping approaches, based on power or momentum conservation, have been proposed for the conceptual design phase[3]. Also, different performance metrics have been introduced, such as the power saving coefficient by Smith[1] or a fuel burn metric by Drela[4].

A previous 2D design space investigation on the BLI-360 configuration has been carried out in [5]. In this work, an analysis of the influence of the main geometrical features of a BLI-360 propulsor – nacelle height and length, fan hub radius – on the engine performance was carried out. One of the primary concerns was the definition of a consistent performance metric.

The choice has been to introduce a figure of merit based on a momentum conservation approach which does not need a precise separation between thrust and drag[6], thus solving the ambiguity in the forces accounting. In order to assess a global performance metric, a Net Assembly Force (NAF) was defined that takes in account all the forces acting on the airframe (Figure 2).

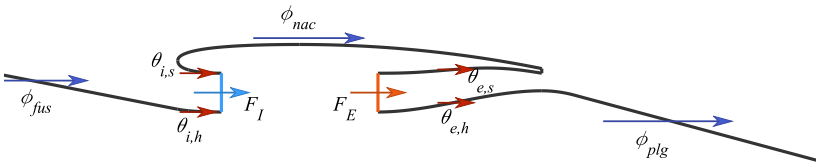

Fig. 2 Streamwise forces acting on the airframe

The wall forces acting on the drag domain on a generic surface A are denoted by ϕ, the ones acting on the thrust domain are denoted with θ, whilst the gauge forces at the intake and exhaust sections of the propulsor are denoted by F:

$$\phi, \theta = \int_{S_w} \left[(p - p_\infty)\, \hat{n} + \vec{\tau}_w \right] \cdot \hat{x} dS \tag{1}$$

$$F = \int_A \left[(p - p_\infty)\, \hat{n} + \rho \vec{V} \left(\vec{V} \cdot \hat{n} \right) \right] \cdot \hat{x} dA \tag{2}$$

The Net Assembly force can therefore be evaluated by taking the sum of the wall and gauge forces. The NAF has been then referred to a reference fuselage drag, which has been provided based on available data on a commercial aircraft:

$$\Delta NAF = NAF - D_{ref} \tag{3}$$

ΔNAF can therefore be intended as a surrogate of the net propulsive thrust, which takes into account the installation effects of the BLI nacelle and the variations in the fuselage shape with reference to a non-BLI configuration. As a consequence, it has been defined a ΔNAF efficiency, which quantify the amount of shaft power converted in useful power, having defined the useful power in relation to ΔNAF (the minus sign is justified by the fact that the NAF has been defined positive in the streamwise direction).

$$\eta_{\Delta NAF} = \frac{W_{\Delta NAF}}{W_{fan}} \tag{4}$$

with:

$$W_{\Delta NAF} = -\Delta NAF\, V_\infty \tag{5}$$

Starting from these performance metrics, the scope of the present activity is to carry out a complete 3-dimensional design of a BLI-360 propulsor with the aim of maximizing the efficiency for a given NAF value. To this end, a sequential approach has been followed:

1) Definition of the 2D axisymmetric parametric model in terms of design variables and shapes;
2) Optimization of the 2D axisymmetric propulsor;
3) Optimization of the 2D nacelle profiles at the azimuthal planes 0, 180deg;
4) Definition of the interpolating laws between the azimuth profiles and 3D parametric analysis.

IV. Two-Dimensional Axisymmetric Optimization

A. Geometric parametrization

The first phase of the design process consisted in the definition of a parametric model defined by appropriate curves and design variables, as shown in Figure 3. The preliminary design is based on a 2D axisymmetric geometry that reproduces the main features of a WTT model for transonic flow conditions ($M_\infty = 0.8$, $Re \sim 3e6$). Thus, the choice of the design variables and their side boundaries were driven by a number of size and manufacturing constraints. The design variables include the axial lengths of the intake and exhaust sections, as well as the passage areas and the external cowl shape. The aft-fuselage has been kept fixed to the one defined for the WTT model. A further design variable is the fan total pressure ratio.

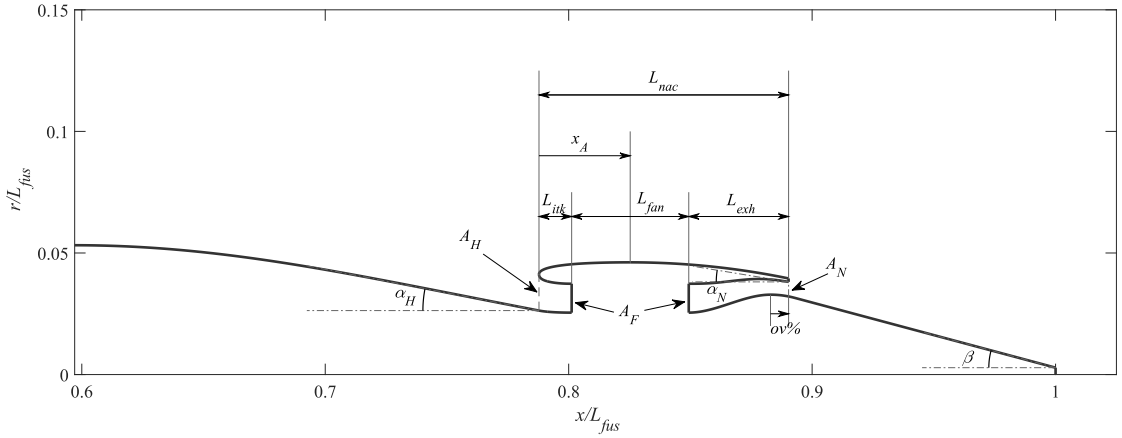

Fig. 3 Parametric 2D model.

The geometry consists of multiple types of curves, all connected with a tangency condition in order to maintain a C^1 class of continuity between all sections comprising the shape. The intake region consists in a parabolic arc defining the hub shape, and a Bézier curve which produces the shroud section. The exhaust region is composed of two 5^{th} order polynomial curves: the hub section is defined by a Bell-Mehta curve, whilst the shroud shape has been created by imposing a non-zero inclination angle at the trailing edge section, which is guided by an opportune design variable.

The external cowl is composed of a Bézier curve defining the lip, and a circular arc from the maximum radius point to the trailing edge. The tail plug is made up of a circular arc smoothing the connection between the exhaust-hub curve and the final straight line, which features a fixed inclination angle β. The fan exhaust and intake sections has been considered equal, in accordance with the WTT model requirements.

The manufacturing and size constraints led to the definition of the following design variables: (a) the ratio between the highlight and the fan areas; (b) the ratio between the nozzle throat and fan areas; (c) the exhaust length; (d) the relative axial position of the maximum radius point with respect to the nacelle length; (e) the inclination angle of the nozzle shroud curve tangent line, normalized between 0 and the external cowl inclination angle at the trailing edge; (f) the nozzle overlap; (g) the nozzle shroud radius point; (h) a set of control points for the internal lip Bézier curve.

Other parameters, such as the intake length, highlight hub radius and inclination angle of the parabolic arc, fan areas and radii, nacelle maximum thickness and the plug curvature radius and inclination angle have been fixed to match the WTT model requirements. The airframe overall length was about 1.5m.

B. Numerical Model

RANS CFD simulations using ANSYS® Fluent have been set up for the evaluation of the fitness functions. In the CFD analyses, a boundary conditions model defined by mass flow outlet/inlet has been used as substitute of an actual fan, in accordance with the preliminary design space investigation[5]. Being the fan polytropic efficiency a functional constraint and the fan pressure ratio a design variable, the ingested mass flow rate becomes a consequence of these parameters and the propulsor cross-sectional areas, thus its value cannot be evaluated prior to the CFD analysis. The

problem has been solved iteratively by fixing the fan pressure ratio and polytropic efficiency as target values and by defining the mass flow rate and exhaust total temperature as:

$$\dot{m}\,(j+1) = A_E\,\pi_c\,p_I^0(j)\sqrt{\frac{k}{R\,T_I^0(j)\,\pi_c^{\frac{k-1}{k\,\eta_{pol}}}}}M_E(j)\left(1+\frac{k-1}{2}M_E^2(j)\right)^{\frac{k+1}{2(1-k)}} \tag{6}$$

$$T_E^0(j+1) = T_I^0(j)\,\pi_c^{\frac{k-1}{k\,\eta_{pol}}} \tag{7}$$

in which the intake section total temperature and total pressure and the exhaust section Mach number are calculated at the end of each CFD iteration and used to re-evaluate the mass flow rate until convergence. The fan model is summarized in the flowchart of Figure 4.

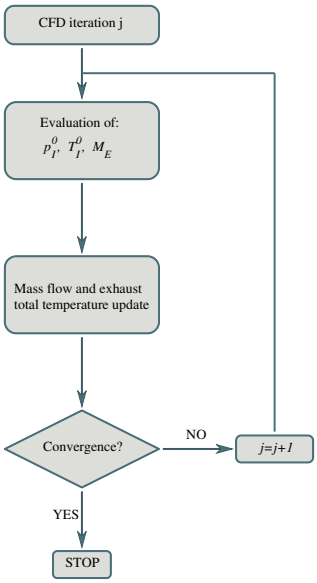

Fig. 4 Flowchart of the fan boundary conditions model.

The parametric mesh was built in Pointwise® based on a semi-structured grid topology. A structured mesh has been used to discretize the region around and within the propulsor and the rear wake, whilst the external flow field has been meshed with an unstructured block. The flow domain extents for $L_x \times L_r = (50 \times 30)L_{fus}$, being L_{fus} the overall fuselage length. The structured wake region extents for $5L_{fus}$. A grid convergence analysis has been carried out in the previous design space investigation [5]. The sensitivity analysis led to the choice of a grid with approximately $660k$ elements, corresponding to the one featuring the lowest values of forces percentage differences with reference to the previous mesh. An average y^+ value of ≈ 0.67 has been achieved. An example of the resulting mesh is presented in Figure 5.

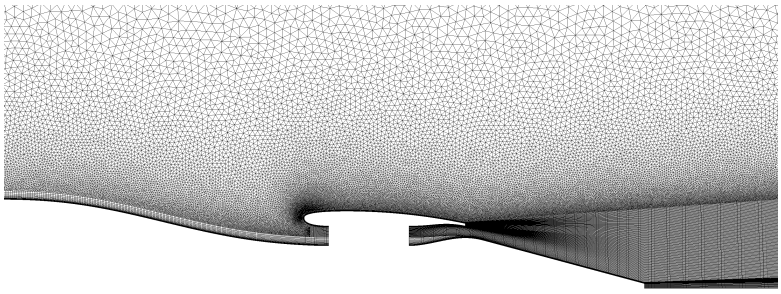

Fig. 5 Parametric mesh topology.

C. Multi-Objective Optimization Problem (MOOP) Formulation and Results

It has been already illustrated [5] that the parameter ΔNAF efficiency takes a meaningful value for a given required Net Assembly Force. Hence, a sensible optimization-wise approach should consist in fixing the required NAF as a functional constraint and search for the individual with a minimum shaft-to-ΔNAF powers ratio (which is equal to a maximum ΔNAF efficiency) for that given NAF. In an optimization point of view, it's also possible to use the NAF in order to obtain a Pareto Front which comprises all the maximum-efficiency individuals for different Net Assembly Forces values. This permits to explore different NAF configurations simultaneously. This has been done by specifying the Net Assembly Force fitness function as a minimization of the NAF value, being this force defined positive in the streamwise direction. The optimization has been formalized as a bi-objective problem, comprising two fitness functions to be minimized:

$$\text{minimize} \quad \boldsymbol{F}(\boldsymbol{dv}) = \left\{ \begin{array}{c} 1/\eta_{\Delta NAF} \\ NAF \end{array} \right\} \tag{8}$$

The algorithm that has been used for the optimization processes is GeDEA-II[7–13], a proprietary tool running in Matlab® environment which treats the genetic diversity as an objective, thus emphasizing both the non-dominated solutions and the most genetically different ones. A first optimization has been carried out considering a starting population of 30 individuals evolving for 25 generations. The results are expressed in an equivalent objective space, presented in Figure 6, in which the fitness functions have been substituted with the performance parameters (being the fitness functions a rearrangement of the efficiency and the net assembly force in a minimization point of view). These parameters have therefore been normalized so that 1 represents the maximum value of $\eta_{\Delta NAF}$ (abscissa) or NAF (ordinate) obtained by the optimization process. Although the Pareto front is highly populated, the region between normalized $NAF \sim 0.3$ and ~ 0.5 is discrete. However, it has been observed that the Pareto Front individuals at the edges of this range feature neglectable geometrical differences, and the differences in terms of NAF solely depend on an increasing in the fan pressure ratio.

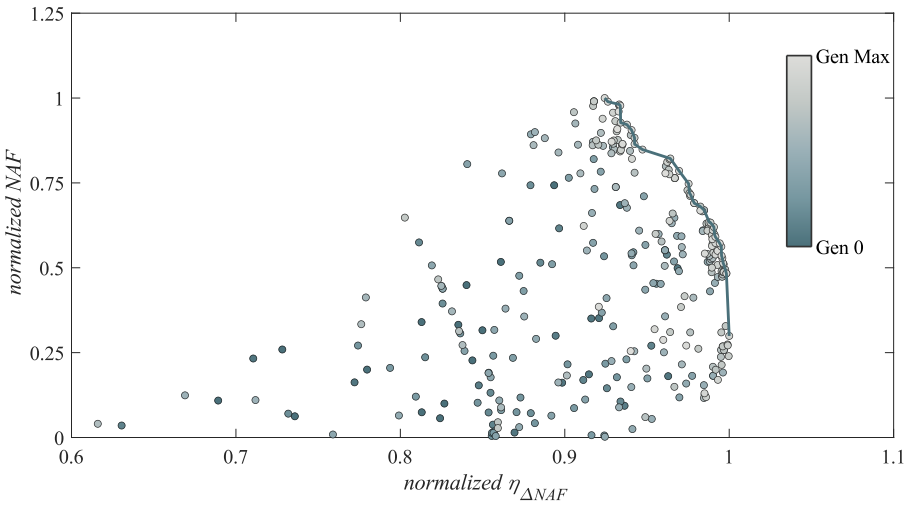

Fig. 6 Optimization results for the axisymmetric case: normalized Pareto front

In accordance with the WTT requirements, two target NAF values have been chosen, and the correspondent individuals in the Pareto Front have been taken as optimal shapes. The optimal individuals have been represented in Figure 7. Slight differences can be observed in the exhaust portion of the propulsor. This is due to the fact that, besides the highlight height and lip shape, the intake section has been constrained.

It is worth noting that although a small degree of freedom in the nacelle lip was maintained, the optimization process led to very similar shapes. The main differences in the exhaust section are guided by the higher throat area required from the Opt2 individual (which corresponds to the highest NAF value). Differences are visible also in the axial position of the maximum radius point of the external cowl, which is slightly downstream in the Opt1 case.

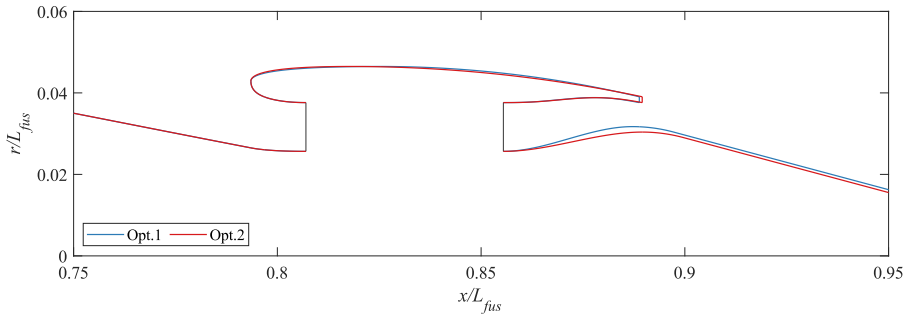

Fig. 7 Optimization results for the axisymmetric case: optimal shapes.

Figures 8 and 9 show the Mach number contours and streamlines of the optima. For both the individuals, similar conclusions can be made. Firstly, the best individuals features short exhaust ducts, which translate in short nacelles (having fixed both the fan and intake axial lengths). Also, although the fan pressure ratio has been constrained between 1.30 and 1.80, the optimal values are $\pi_c = 1.37$ for Opt1 and $\pi_c = 1.40$ for Opt2. These observations are in line with the results of the preliminary design space analysis[5]. Another interesting observation concerns the absence of a throat section at the intake region, although the lip control points distribution could have produced such configuration. This leads to a convergent duct upstream the fan, thus an acceleration of the ingested flow. Such acceleration is more prominent for the Opt2 case, which ingests a higher mass flow than Opt1.

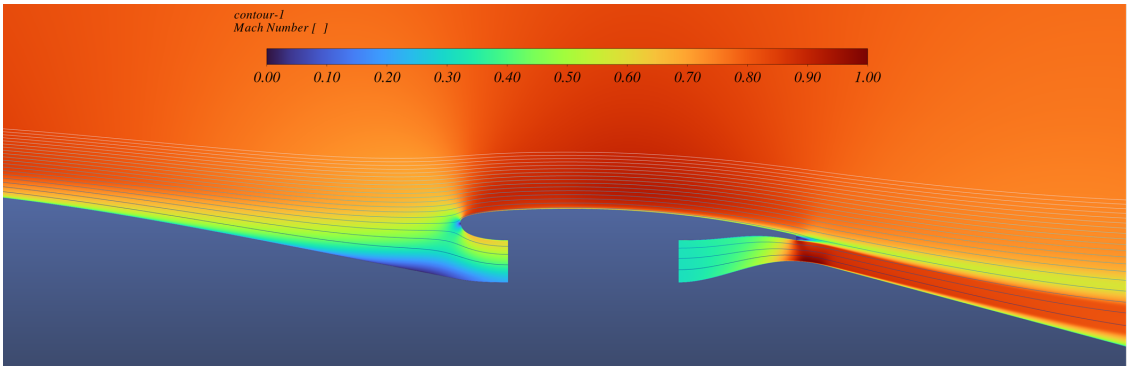

Fig. 8 Invididual Opt1: Mach number contour and streamlines.

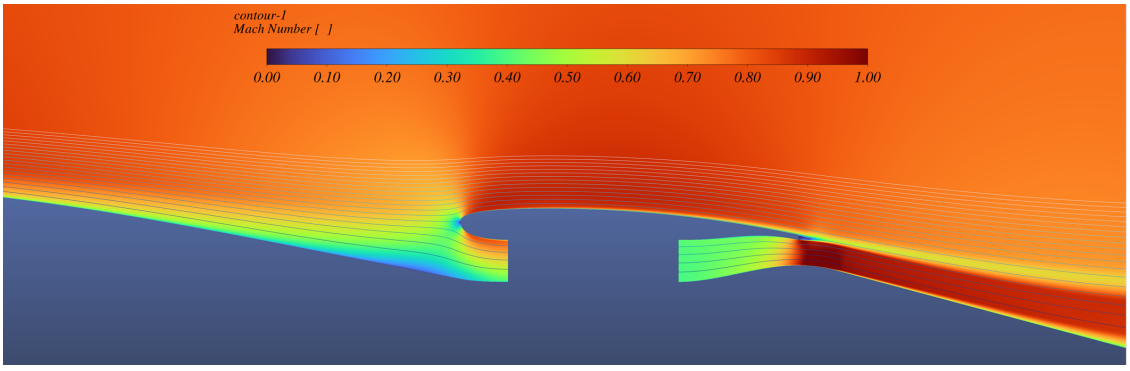

Fig. 9 Invididual Opt2: Mach number contour and streamlines.

V. Three-Dimensional Design and Analysis

In Section IV, the optimization process of the 2D axisymmetric propulsor has been treated. The results served as a base for the three-dimensional design of the WTT model propulsor.

A. Definition and Optimization of the Azimuth Profiles

The design phased started with assuming that the optimized axisymmetric propulsor should consist in the profile at an azimuth plane of $90deg$. Thus, the choice has been to refine the optimal shape for the azimuthal profiles at 0 and $180deg$. In this process, the majority of the 2D design variables have been constrained: the exhaust axial length, as well as the nozzle throat (area, inclination of the shroud surface, overlap, hub radius) have been set to the 2D optima values, whilst the target of the shape refinement have been the highlight height and the axial position of the cowl maximum radius point. The fan total pressure ratio has been also constrained.

The azimuth profiles optimizations have been carried out in the hypothesis of axisymmetric flow. For each azimuth, the aft-fuselage has been defined starting from the fixed reference shape of the WTT model, and a revolution of the geometry around the propulsor axis has been considered. The mesh topology and size has been kept coherent with the one of the preliminary optimization, as well as the CFD model and the MOOP formulation, which is analogue to the previous optimization (expressed in equation 8). Although the formulation permits to obtain individuals with different Net Assembly Forces, the focus was the maximization of the ΔNAF efficiency. Having considered different fuselage shapes (in terms of maximum radius and aft-fuselage profiles) for the 2 azimuth planes, a discrepancy in terms of evaluated net assembly force in axisymmetric conditions had to be expected. Nevertheless, such discrepancies are to be considered systematic in the performance evaluations of the individuals, therefore an improvement in the efficiency can be considered a valid result.

The optimizations have been carried out for both Opt1 and Opt2 separately, for a total of 4 runs in total (2 for each optimum, and for each optimum 2 azimuth planes have been considered). The choice is justified by two considerations:

- Different azimuth planes produce different reference fuselages. This precludes the possibility to run a single optimization which could consider both the azimuth cases.
- Such optimization processes are to be considered as refinements of the optimal individuals found in the preliminary analysis. Therefore it has been more convenient to start from such geometries and searching for the optimal shapes individually rather than in a single optimization for both the optima.

The optimization results are presented in figures 10 and 11 in terms of normalized Pareto Fronts. The optimal individuals lying in the Pareto fronts feature very similar efficiency values. A more pronounced variation is observable in the Net Assembly force for the 180deg azimuth cases, but within a 5% range. Such small differences between the individuals led to the choice of the optimal shape in terms of maximum efficiency.

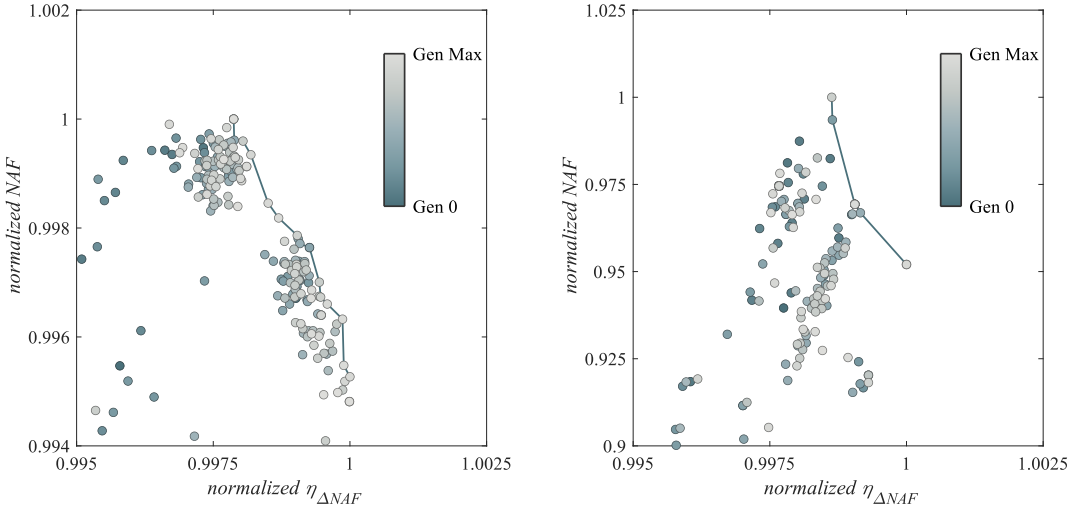

(a) Pareto Front of Opt1, azimuth 0deg **(b) Pareto Front of Opt1, azimuth 180deg**

Fig. 10 Optimization results for Opt1.

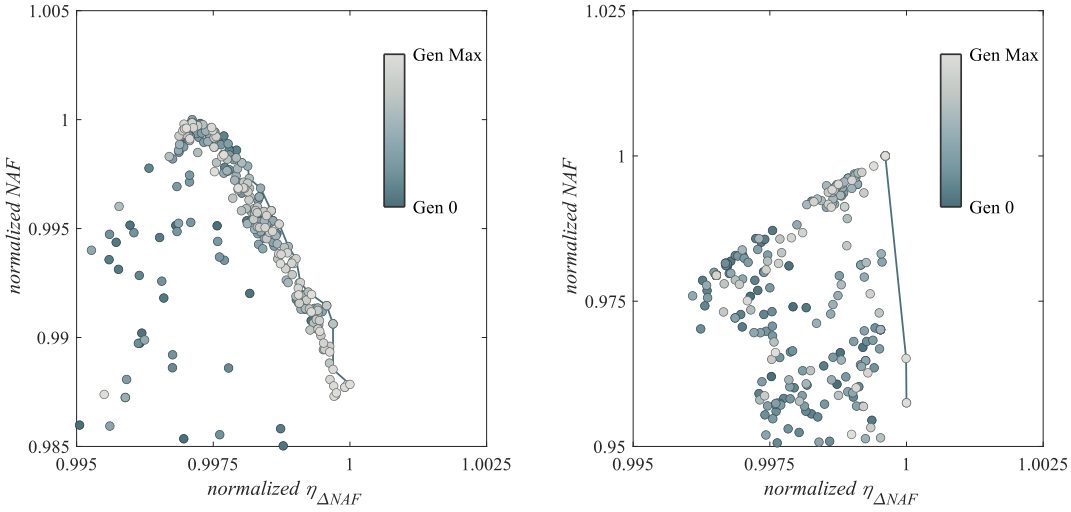

(a) Pareto Front of Opt2, azimuth 0deg **(b) Pareto Front of Opt2, azimuth 180deg**

Fig. 11 Optimization results for Opt2.

It is interesting to note how the optimizations followed a similar trend in both the individuals: the profiles corresponding to the azimuth 0 feature a decreasing in the highlight height and a displacement of the maximum cowl radius point towards the nacelle trailing edge. On the other hand, the 180deg profiles feature an increasing in the highlight height and no displacement with reference on the 90deg profiles. Figure 12 shows both the shapes and the isentropic Mach Number profiles of the Opt2 optimized profiles at the two azimuth planes.

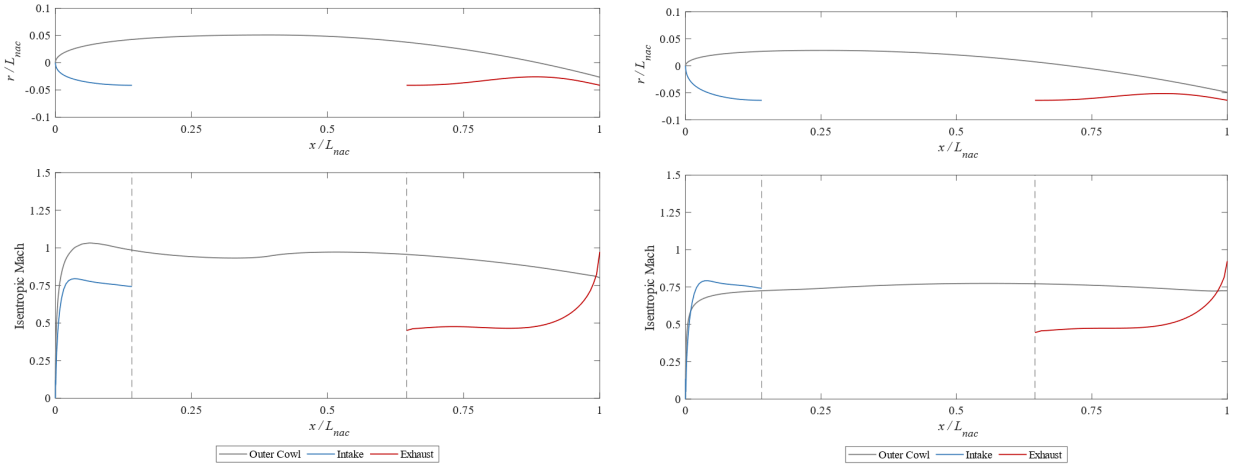

(a) Profiles at azimuth 0deg **(b) Profiles at azimuth 180deg**

Fig. 12 Isentropic Mach Number profiles of Opt2.

To summarize, the main outcomes of the profiles refinement process are the following:

- The highlight height is an increasing function of the azimuth angle, varying from 0 to 180deg. This can be justified by the fact that the upper profile (azimuth 0) is invested by a faster flow than the one of azimuth 180deg. Having fixed the fan pressure ratio and the exhaust areas, being the nozzle in choking conditions the ingested mass flow rate is substantially fixed. Therefore, a smaller intake area is needed to ingest the same mass flow rate at azimuth 0. Vice versa, the tendency is to increase the intake area when the flow is slower.
- The azimuth 0 profiles feature a clear displacement of the maximum cowl point towards the nacelle trailing edge. This is justified by observing the isentropic Mach number profiles: as previously stated, the upper profile is

invested by a faster flow. The displacement seems necessary in order to prevent - or minimize - the occurrence of a supersonic region at the external cowl lip. This occurrence is not observed for the azimuth 180deg profile, which features the same axial position of such point.

B. Definition of the Azimuth Interpolation Laws and 3D Model

The optimization process and subsequent shape refinement served as a preliminary design phase for the definition of the actual 3-dimensional model. The rationale behind the choice of a 2D design process has been to reduce the overall computational effort with respect to a complete 3D design based on an optimization. However, the following parametric analysis had to be carried out in order to determine the azimuthal laws connecting the optimal shapes at the different azimuth angles. Specifically, the 3D design followed a sequential approach which can be summarized in these steps:

1) Definition of appropriate azimuth laws of the three profiles, aimed at the CAD and CFD model parametrization.
2) Parametric analysis on the azimuth laws, aimed at determining their influence on the propulsors performance.

For each of the two optimal individuals, the design variables that have been kept constant for the azimuth refinement determined three profiles that share the following common geometrical features: (a) axial lengths (intake, fan, exhaust); (b) exhaust duct and plug shapes. The differences among the azimuth profiles consist in the highlight heights and the axial positions of the max. radius cowl point, which lead to slight differences in the external cowl and intake lip shapes. Therefore, two azimuth laws had to be defined in order to properly interpolate the three profiles.

The main concern regards the mathematical conditions that should be given to such curves: being the propulsor symmetric with respect to the 90deg azimuth plane, it is important to maintain the first derivative equal to zero in correspondence of the azimuth 0, 180deg profiles. Furthermore, being the maximum radius point of the external cowl equal for the 90 and 180deg azimuthal planes in both cases, it has been decided to rely on a polynomial curve for the definition of the cowl law between 0 and 90deg. On the other hand, the second portion of the azimuthal law consists in a constant value. A further condition that has been decided to impose has been a zero-curvature condition at the azimuth 0 and 90deg. The choice is justified by the fact that the 90-to-180 portion has been kept constant, therefore it doesn't feature any curvature.

By imposing such condition on the polynomial curve at the interconnection, it has been possible to define a C^2 class of continuity law. The imposition of the passage through the edges, as well as zero-derivative and zero-curvature conditions at the starting end ending points suggests a curve which resembles a Bell-Mehta polynomial. It has therefore decided to start from the definition of a 5^{th} degree Bell-Mehta curve, and imposing a further condition: such polynomial is characterized by having the mean-ordinate point lying in the mean-abscissa coordinate. The choice has been to define the passage through a point which could impose a displacement of the mean-ordinate coordinate from the average abscissa, as can be seen in Figure 13. In mathematical terms, a total of 7 conditions are to be defined in order to obtain such curve, leading to a 6^{th} degree polynomial: (a) passage through the edges (2 conditions); (b) zero derivative at the edges (2 conditions); (c) zero curvature at the edges (2 conditions); (d) passage through the parametric point (1 condition).

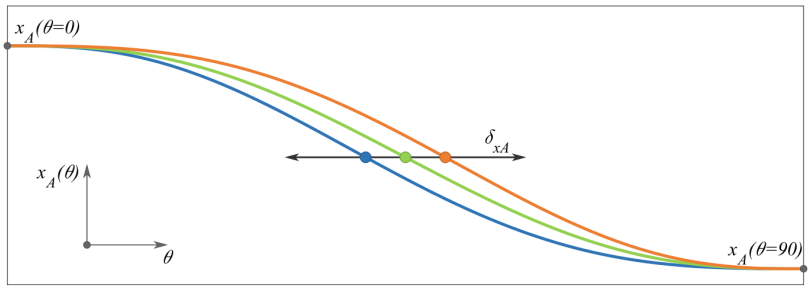

Fig. 13 Maximum cowl radius axial coordinate parametrization.

The highlight radius has been parametrized using two Bezier Curves, both defined by 4 control points, as seen in Figure 14. Considering Figure 14b, the blue curve guides the azimuthal law from the 0deg to the 90deg plane, whilst the red one guides the law from 90 to 180deg. Figure 14a shows in detail the geometric parametrization of the Bezier profile: for both the sections, the constrained points correspond to the curve ends, in which the azimuth values and the highlight radii are known. The central control points have been defined so that they could grant continuity with

tangency between the portions. Therefore, P_2 has been freed to move horizontally, whilst P_3 has been freed vertically. Both the points have been parametrized by normalized design variables denoted in the figure as δ_i.

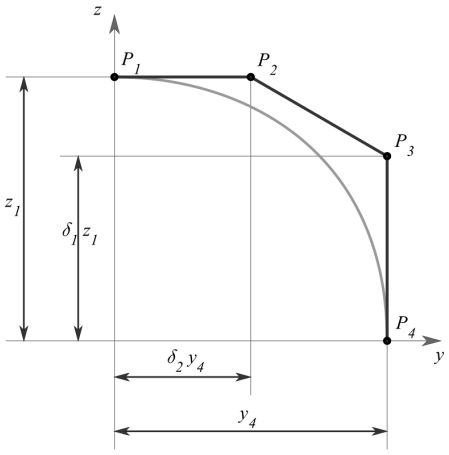

(a) Design variables of the highlight azimuthal law.

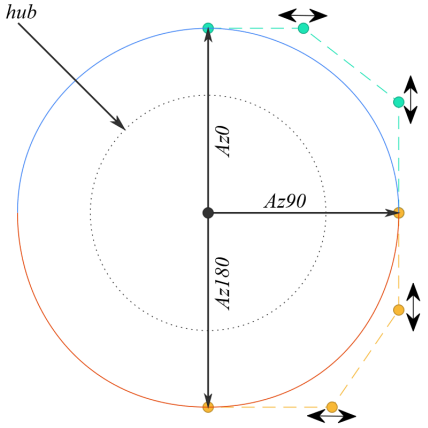

(b) Sketch of the highlight azimuthal profile.

Fig. 14 Highlight interpolation law.

Figure 15 shows the parametric model, in terms of curves (15a) and CAD (15b). The CAD model has been produced via parametric macro using Catia.

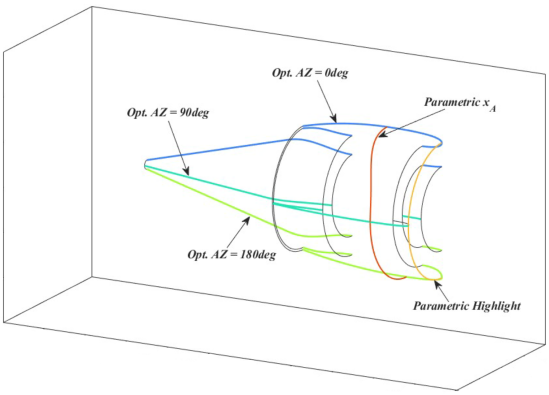

(a) Parametric curves.

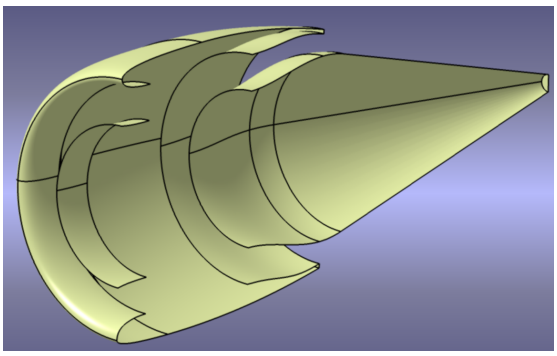

(b) Parametric CAD.

Fig. 15 Parametric 3D model.

C. Azimuth Laws Parametric Analysis

The parametric analysis has been carried out for both Opt1 and Opt2. The design variables that have been considered are: (a) the normalized parameter δ_{xA} which guides the displacement of the mean-ordinate coordinate of the cowl radius law; (b) four normalized parameters ($\delta_{y,u}$, $\delta_{z,u}$, $\delta_{y,l}$, $\delta_{z,l}$) which guide the Bézier curves (upper, lower) control points of the highlight interpolation law. A set of individuals has been created using a Latin Hypercube Sampling. It is important to highlight that the side boundaries to the design variables provided a quite tight design space. This has been necessary in order to obtain feasible geometries, mainly for two reasons: (1) great displacements in the mean-x_A point would have produced polynomial curves featuring maxima or minima between the end points. This is due to having considered a 6^{th} degree polynomial. (2) great displacements in the highlight control points might have determined highlight curves which could locally feature higher radii than the maximum height cowl point, or lower than the fan intake section.

The results are presented in Figures 16 and 17 in terms of correlation plots: each row represents a design variable, whilst the columns show the forces acting on the various portions of the airframe, the Net Assembly force and the ΔNAF efficiency. The circle dimension and color intensity represent the coupling level between parameters: the red color corresponds to a positive correlation, while the blue color corresponds to a negative one.

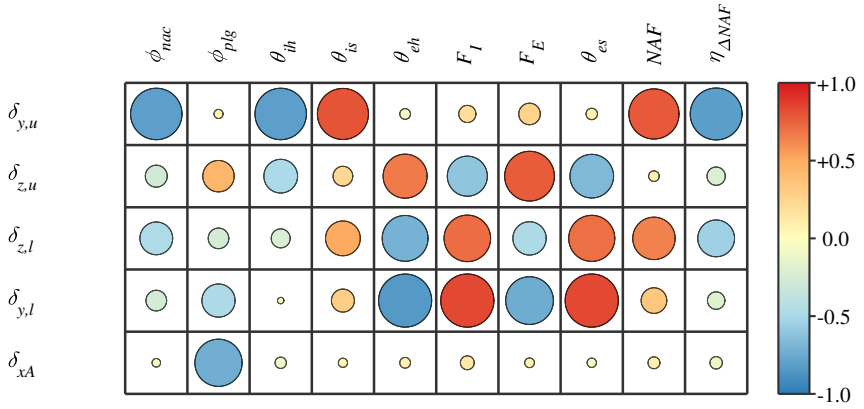

Fig. 16 Correlation plot of the azimuthal laws influence on Opt1.

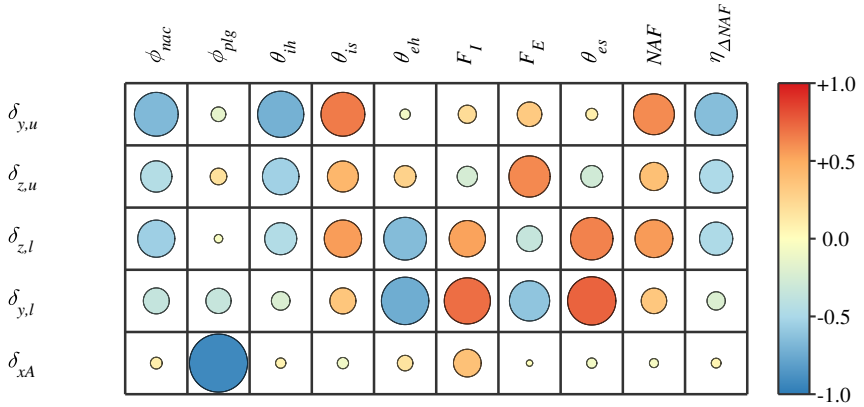

Fig. 17 Correlation plot of the azimuthal laws influence on Opt2.

At first glance, all the design variables have an influence in the forces components. Furthermore, similar correlations can be observed in the two cases. The outer cowl maximum radius position (represented by δ_{xA}) has the lowest influence on the performance parameters, which are more sensible to the highlight parametrization.

Nevertheless, it has been observed that, although the correlation between the design variables and performance metrics are rather clear, the variations in terms of performances are relatively small. Opt1 features a maximum variation of efficiency (between the minimum efficiency and the maximum one observed in the population) of 1.096%. Opt2 shows a maximum variation in the efficiency of 0.725%. This is consistent with the fact that the design space has been highly constrained for manufacturing requirements prior to the preliminary 2D design, thus leading to similar azimuthal shapes which, as consequence, have given a small room for refinement in terms of azimuthal interpolations. The Net Assembly Force maximum variation within the populations are 9.153% for Opt1 and 2.905% for Opt2, which are more appreciable. As definitive shapes for the WTT model, it has been chosen for each individuals the one featuring the maximum efficiency value.

Figures 18 and 19 show the Mach number contours at the symmetry plane and at two traverse planes, the first one being the fan intake section and the second one intersecting the nacelle near the maximum cowl radius. From Figure 18 it is apparent how the Mach distributions at azimuth 0 and 180deg are in line with the isentropic Mach number contours of Figure 12, although the cowl profiles have been determined in axisymmetric conditions.

The faster flow at the upper side of the propulsor determines a higher Mach number region at the outer cowl and at the intake, thus determining a circumferential contribute to the inlet flow distortion, which also features a clear radial contribute. The numerical characterization of the flow distortion upstream the fan has not been a part of the design phase, but it is rather clear how a further refinement should take in account a minimization of such flow characteristic.

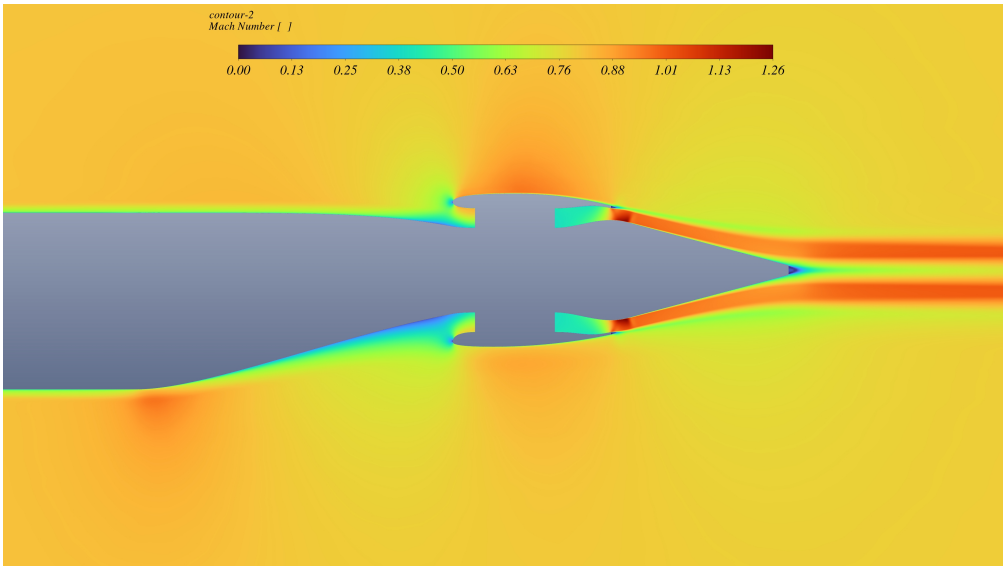

Fig. 18 Opt2 Mach contour at the propulsor symmetry plane.

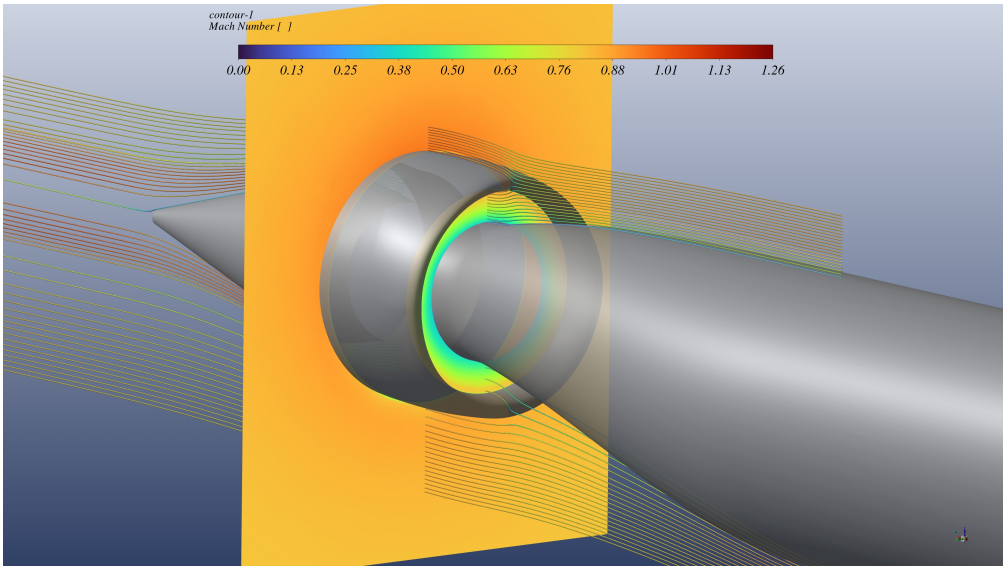

Fig. 19 Opt2 Mach contour at traverse planen and streamlines at the symmetry plane.

VI. Conclusion

The present work is part of the Clean Sky 2 project SUBLIME, and it describes the shape optimization activities carried out for the definition of a BLI-360 WTT model, based on a consistent performance metric for the performance evaluation. A sequential approach has been followed, starting from a simplified 2D axisymmetric case, which has been kept as a reference for the 3-dimensional shape refinement at opportune azimuth angles.

An analysis of the influence of interpolation laws which connect the azimuth shapes has been also produced, and showed little variations in terms of performance. This is mostly caused by the high level of constraints which have been imposed for manufacturing drivers.

The preliminary 2D optimization has given some insight on the geometrical tendency of the nacelle:

- The optimization results show that shorter exhaust ducts are preferable, most likely because reducing the axial length of the propulsor also reduces the external cowl wetted area, which in turn reduces the nacelle drag contribute;
- The optimal individuals do feature a neglectable overlap of the nacelle over the tail plug.
- The nozzle exhaust radius tends to settle at values in proximity of the fan exhaust shroud radius, thus lowering the hub and reducing the tail plug wetted area. This also produces more cambered cowls.
- The optimal individuals feature almost identical intake profiles. Although the axial length has been constrained, the highlight radius and the curve profiles are very similar, and the lack of a throat section can be observed. As a consequence, the tendency is to accelerate the ingested flow towards the fan.
- The fan total pressure ratios are similar for the two optimized shapes and coherent with the results observed in the design space investigation. Opt2 features a higher exhaust area and ingested mass flow, which lead to a higher NAF.

From the 2D optimization of the 0 and 180deg azimuthal planes the following conclusions can be drawn:

- The highlight height tends to be an increasing function of the azimuth angle (from 0 to 180deg).
- The outer cowl maximum radius point at the 0deg azimuthal plane tends to settle downstream. This seems to prevent the occurrence of a supersonic region at the external cowl lip: at the 0deg azimuthal plane, the profile is locally less submerged, thus being invested by a faster flow. This tends to produce a higher isentropic Mach number at the outer cowl. Thus, the displacement of the max radius point axial position downstream is justified by the tendency of decreasing the maximum isentropic Mach number.

The 3-dimensional geometries feature a slight decrease in the efficiency if compared to the 90deg 2D case – which is to be considered as a mean azimuthal plane. This was actually expected, since the 2D optimizations have been carried out at axisymmetric conditions, therefore they did not consider the 3-dimensional effects of the (a) aft-fuselage upsweep and (b) the azimuthal interpolation laws among the nacelle profiles.

The azimuthal laws seem to feature a very low influence over the ΔNAF efficiency: this is most likely caused by the strong set of geometrical constraints that have been defined on the WTT model. A further shape refinement should take into account the inlet flow distortion.

Acknowledgments

This study is financed by the Clean Sky 2 project SUBLIME (Supporting Understanding of Boundary Layer Ingestion Model Experiment). The project has received funding from the European Union's Horizon 2020 research and innovation programme under grant agreement number 864803.

References

[1] Smith, L. H., "Wake ingestion propulsion benefit," *Journal of Propulsion and Power*, Vol. 9, No. 1, 1993, pp. 74–82. https://doi.org/10.2514/3.11487, URL https://doi.org/10.2514/3.11487.

[2] Menegozzo, L., and Benini, E., "Boundary Layer Ingestion Propulsion: A Review on Numerical Modeling," *Journal of Engineering for Gas Turbines and Power*, Vol. 142, No. 12, 2020. https://doi.org/10.1115/1.4048174, URL https://doi.org/10.1115/1.4048174, 120801.

[3] Habermann, A. L., Bijewitz, J., Seitz, A., and Hornung, M., "Performance bookkeeping for aircraft configurations with fuselage wake-filling propulsion integration," *CEAS Aeronautical Journal*, Vol. 11, 2020, pp. 529–551. https://doi.org/10.1007/s13272-019-00434-w.

[4] Drela, M., "Power Balance in Aerodynamic Flows," *AIAA Journal*, Vol. 47, No. 7, 2009, pp. 1761–1771. https://doi.org/10.2514/1.42409, URL https://doi.org/10.2514/1.42409.

[5] Battiston, A., Ponza, R., and Benini, E., "Design Exploration for an Axisymmetric Rear BLI Propulsor," *AIAA Propulsion and Energy 2021 Forum*, 2021. https://doi.org/10.2514/6.2021-3470, URL https://arc.aiaa.org/doi/abs/10.2514/6.2021-3470.

[6] Hendricks, E. S., "A Review of Boundary Layer Ingestion Modeling Approaches for use in Conceptual Design," *NASA Technical Reports Server*, 2018. URL https://ntrs.nasa.gov/citations/20180005165.

[7] Toffolo, A., and Benini, E., "Genetic Diversity as an Objective in Multi-Objective Evolutionary Algorithms," *Evol. Comput.*, Vol. 11, No. 2, 2003, p. 151–167. https://doi.org/10.1162/106365603766646816, URL https://doi.org/10.1162/106365603766646816.

[8] Ronco, C., and Benini, E., "GeDEA-II: A Simplex Crossover Based Evolutionary Algorithm Including the Genetic Diversity as Objective," *Applied Soft Computing*, Vol. 13, 2013, pp. 2104–2123. https://doi.org/10.1016/j.asoc.2012.11.003.

[9] Toffolo, A., and Benini, E., "A new pareto-like evaluation method for finding multiple global optima in evolutionary algorithms," *Late Breaking Papers at the 2000 Genetic and Evolutionary Computation Conference*, 2000, pp. 405–410.

[10] Comis Da Ronco, C., Ponza, R., and Benini, E., "Aerodynamic shape optimization of aircraft components using an advanced multi-objective evolutionary approach," *Computer Methods in Applied Mechanics and Engineering*, Vol. 285, 2015, pp. 255–290. https://doi.org/https://doi.org/10.1016/j.cma.2014.10.024.

[11] Benini, E., Ronco, C., and Ponza, R., "Aerodynamic Shape Optimization in Aeronautics: A Fast and Effective Multi-Objective Approach," *Archives of Computational Methods in Engineering*, Vol. 21, 2014, pp. 189–271. https://doi.org/10.1007/s11831-014-9123-y.

[12] Massaro, A., and Benini, E., "A Surrogate-Assisted Evolutionary Algorithm Based on the Genetic Diversity Objective," *Applied Soft Computing*, Vol. 36, 2015, pp. 87–100. https://doi.org/10.1016/j.asoc.2015.06.026.

[13] Benini, E., Venturelli, G., and Łaniewski, W., "Comparison between pure and surrogate assisted evolutionary algorithms for multiobjective optimization," *Front. Artif. Intell. Appl*, Vol. 281, 2016, pp. 229–242.